DEFECT RECOGNITION AND POWER LOSS ESTIMATION OF PV SYSTEMS USING INFRARED THERMOGRAPHY

Bjørn L. Aarseth[1*] and Erik Stensrud Marstein[1,2]
[1]Department of Technology Systems, University of Oslo,
Gunnar Randers vei 19, 2007 Kjeller, Norway
[2]Institute for Energy Technology,
Instituttveien 18, 2007 Kjeller, Norway
*e-mail: b.l.aarseth@its.uio.no

This study investigates how thermal signatures observed in PV systems using *infrared thermography* (IRT) affect the performance of PV modules and strings. To assess this, we use IRT images as a basis for circuit modeling of modules with defected solar cells. This allows us to calculate the performance of the individual modules with thermal signatures and the module string. We model the IV characteristics of defective modules based on IRT images and fit the results to field IV traces of the imaged modules. By IRT imaging, several thermal signatures have been identified, and by using a portable IV tracer, the power loss related to each defect under the given conditions has been found. Information from the IRT images are used as input to a model we have developed for defect evaluation, and a comparison of model and IV tracer data for a range of defective solar modules is presented. The string modeling shows that the power loss from a given thermal signature is highly dependent on string length and circuit design. For string sizes larger than 20 modules, only defects that affect two or more module substrings are expected to give a power loss higher than 3%.
Keywords: PV system, PV module, Degradation, Infrared Thermography

1 INTRODUCTION

Infrared thermography (IRT) has been proven to be an efficient method for robust condition monitoring of an active PV system, and is widely accepted as an important tool for *operation and maintenance* (O&M) of *photovoltaic* (PV) systems [1], [2]. It allows for reliable detection of hotter areas within a module, often referred to as thermal signatures. Still, the knowledge about how a given thermal signature in a module affects the output power of the system is limited. By extension, this also means that whether a module containing a thermal signature should be replaced or not is unclear. The outcome of an inspection should be a direct course of action for the operator, with specific action points, including a list of modules to be replaced, and which strings should be more carefully monitored to allow for faster recognition of anticipated failures. An integral part of such a course of action is understanding the impact of the thermal signatures on output power, as power loss is usually one of the top priorities of a plant operator.

In addition to IRT, production data analysis is often used for monitoring the state of the plant. This potentially allows for continuous online detection of power loss. The production data, however, normally contains significant noise, which reduces the sensitivity for reliable failure detection [3], [4].

In this study, IRT has been used to identify faulty modules in an 8-year-old ~88 kW_p system consisting of 400 multicrystalline silicon modules. The system is deliberately built with modules that did not pass quality control after production, making it a unique location for investigating PV modules containing thermal signatures, a task that would otherwise require a significantly larger sample volume. The *Current-Voltage* (IV) characteristics of modules containing different thermal signatures were investigated using field IV tracing. A circuit model was fitted to the measured IV curves, allowing for simulations of how different thermal signatures affect the power generation of an arbitrary system design.

2 METHODS

2.1 Infrared Thermography

The thermal images are acquired with an Optris PI 640 LW infrared camera with a resolution of 640x480 pixels, a frame rate of 32 Hz and a 33x25 degree field of view lens. An emissivity value of 0.85 is used for the glass surfaced modules according to Ref. [5]. All images of the study were taken under clear-sky conditions with an in-plane irradiance >800 W/m^2. In parallel with the IRT imaging, visual inspection was done on modules showing thermal signatures.

2.2 Current-Voltage Measurements

A Tritec TRI-KA portable IV tracer (voltage and current uncertainty of < ±1 %) together with a TRI-SEN portable irradiance (uncertainty ±5 %) and module temperature sensor (uncertainty ±3 %) were used for the field IV measurements. IV measurements were made on the same clear sky days as IRT imaging, i.e. under high irradiance and stable conditions. Because of slight variations in in-plane irradiance and module temperature between measurements, however, all the IV curves have been converted to *Standard Test Condition* (STC) values using correction procedure 2 in Ref. [6], for better comparison. Datasheets were not available for the non-quality approved modules, hence coefficient values used in the calculation were α_{rel} = 0.02 %/K, β_{rel} = -0.4 %/K, B = 0.05, R_s'= 0, and κ' = 0. That the IV measurements of the defective modules can be corrected to STC is an approximation. It has previously been shown that IV characteristics are dependent on temperature [7], consequentially some of these defects might have a different impact on the IV curve at a module temperature of 25 °C. The potential error of the approximation remains to be evaluated.

It should be noted that because this PV plant consists of non-quality approved modules, the modules were not binned into narrow power bins, as is standard for normal installations. This means that modules are mismatched,

and that comparing modules with and without thermal signatures can only be done qualitatively, with potentially large errors.

2.3 Circuit Modeling

The circuit modeling was done using the MATLAB Simulink software [8]. A circuit model of a 60-cell module with three bypass diodes was established, consisting of 60 Simulink Simscape solar cells and 3 bypass diodes. The general Simulink configuration parameters are displayed in Table 1a). For the solar cells, a five parameter equivalent circuit (single diode) was chosen. The model parameters are the diode saturation current (Is), solar-generated current (Iph0 model), irradiance (Ir0), quality factor (N) and series resistance (Rs). Because the IV measurements were corrected to STC, Ir0 was pre-set to 1000 W/m^2, and for simplicity N was set to 1. The material constants used in the model are listed in Table 1b). The measurement and simulation temperature were both set to the STC temperature (25 °C). A variable load was used to scan through the IV curve of the system.

The bypass diodes were modeled using a piecewise linear model, with the constants shown in Table 1c). The piecewise linear model approximates the diode to a linear resistor with two modes: (1) low resistance (on resistance) when the voltage across the diode is larger than the on voltage, or otherwise (2) high resistance (low off conductance). Low values for the forward voltage and on resistance, as well as a low value for the off conductance, were chosen deliberately, to reduce the impact of the bypass diode on the IV characteristics as much as possible.

Three defect types were imitated to model the thermal signatures: (1) a reduction factor in irradiance (Irradiance x reduction factor = effective irradiance on the cell) was applied to imitate a cell crack [9], (2) a shunt resistance that shorted the defective cells with a given resistance was input, and (3) additional series resistance was applied to imitate bad contacts in the junction box and in solder bonds.

Table 1: List of parameters utilized in the MATLAB Simulink simulations, a) the Simulink start, stop, load ramp rate and solver options, b) the material constants of the solar cells, and c) the constants for the piecewise linear diode model used to model the bypass diodes.

a) Simulink configuration parameters	
Start - stop time	0 - 1000
Variable load ramp rate	2 Ω/t
Solver type	Variable step
Solver	Ode15s (stiff/NDF)
b) Solar cell material constants	
Band gap (EG)	1.11 eV
Measurement T	25 °C
Device simulation T	25 °C
c) Piecewise linear bypass diode constants	
Forward voltage	0.026 V
On resistance	0.003 Ω
Off conductance	1e-8 Ω^{-1}

3 RESULTS

3.1 Infrared Thermography

IRT inspection of the PV plant leads to the detection of 18 modules with thermal signatures. Fig. 1 shows modules (A)-(H). Here (A) is a reference module without a thermal signature, while (B)-(H) show representative images of observed thermal signatures. A common way to classify thermal signatures is to categorize them based on their shape. One set of categories, adapted to the thermal signatures observed in this work from Ref. [10] are seen in Table 2.

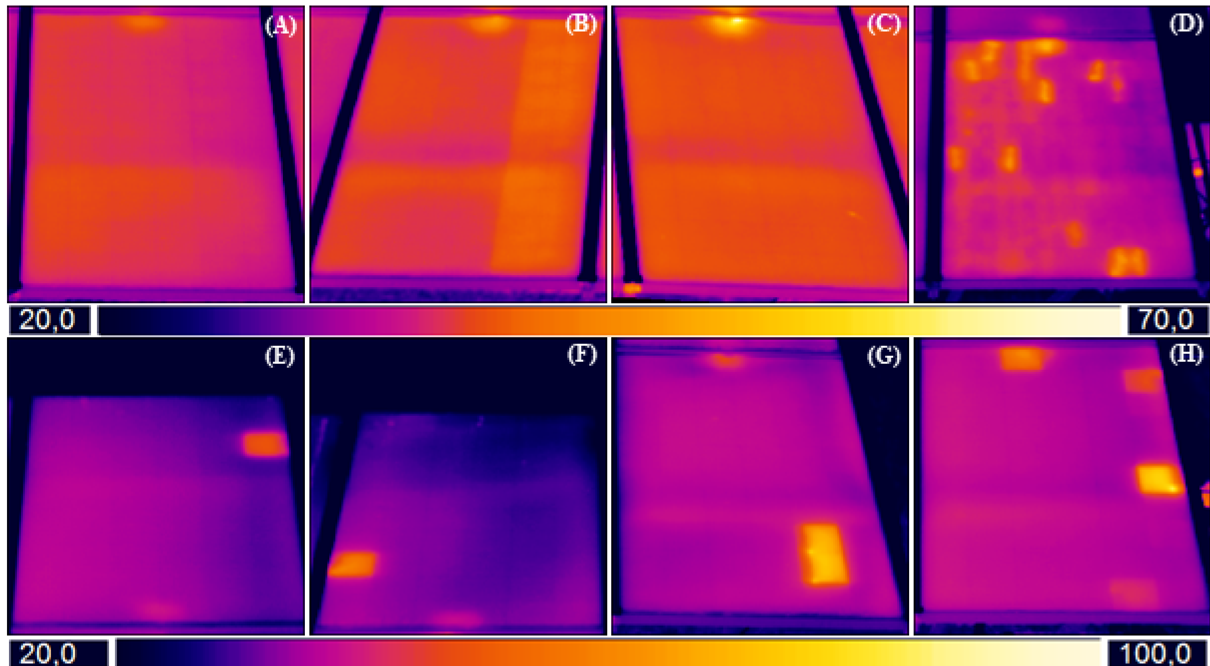

Figure 1: IRT images of 8 selected modules in the system. The thermal signatures presented are (A) no thermal signature, (B) uniformly hot module substring, indicating an active bypass diode, (C) hot junction box, (D) broken front glass, (E) hot cell, (F) hot part of a cell, (G) hot parts of two cells and two hotter points, (H) three uniformly hot cells at different temperatures and a part of a cell with a hotter point.

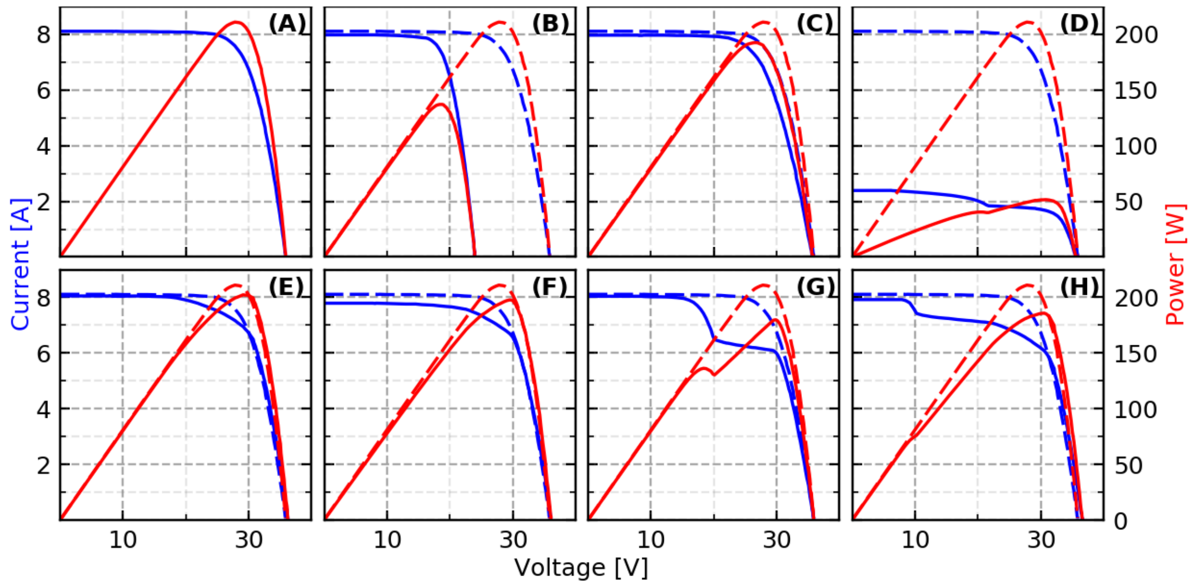

Figure 2: Field IV measurements of all the 8 modules (A)-(H) from Fig. 1. (A) has no thermal signature andis plotted as a dashed line along with the other curves as a guide for the eye. (B) has an active bypass diode, which is reflected in the IV with a 1/3 loss in voltage and power. (C) hot junction box – a slightly less steep slope from Voc to Vmpp, indicating an increase in series resistance. (D) Broken front glass – 3/4 reduction in current and power. (E) Linear loss of current within substring indicating shunt. (F) Similar to (E). (G) Large step in IV curve, indicating isolated area in cells. (H) Step and shunt.

Table 2: Thermal signature categories adapded from [10].

Thermal signature category			
T1	Whole cell hot	**T4**	Hot module substring
T2	Part of cell hot	**T5**	Hot junction box
T3	Point in cell hot	**T6**	Broken front glass

In Fig. 1, module (B) displays a uniformly hot substring (category T4), indicating an active bypass diode; (C) a hot junction box (T5), usually attributed to bad contacts; (D) has a broken front glass (T6); and (E) a whole cell hot (T1). There (perhaps excluding (D)) is little room for subjective interpretations of the thermal signatures for modules (A)-(E).

This is not the case for modules (F), (G) and (H). (F) might fit into category T2 and T1. It has a temperature gradient within the cell from the top left quadrant to the rest of the cell of ~14°C, (from 44°C to 58°C), while the nearby cells have a temperature of 34°C. Due to the rest of the cell being 12°C hotter, and silicon having a high thermal conductance, a colder zone on a cell indicates that the heating originates from a different part of the cell. (G) is easier to categorize. It has a clear step in the IRT where about 25% of two cells are colder than the remainder of the cells. They have a sharp increase in temperature of about 22°C, making it a candidate for T2. The two cells, however, also have a hot point (~1-4°C hotter than the rest of the cells) in the one of the cell solder bonds, which makes the defect a candidate for T3 as well. Module (H) has three cells which can be categorized as T1, while the fourth hot cell could be classified as both T2 and T3. The step gradient within the cell is of the same magnitude as for (G), but the hot point heating is about 10°C hotter than 75% of the cell, making T3 more pronounced here.

It should be noted that T6 can pose a health and safety risk as electrical insulation of the module can be compromised.

3.2 Current-Voltage field measurements

IV measurements of the modules (A)-(H) are shown in Fig. 2, with the same labeling as in Fig. 1. The IV measurement of module (A) is given as a dashed line in all the other plots, as a guide for the eye. Module (B) exhibits a ~33% drop in voltage, expected due to the activated bypass diode and corresponding drop in power. The hot junction box in (C) introduces extra series resistance, seen as the change in slope from the *open circuit voltage* (Voc) to the *maximum power point* (Mpp), slightly reducing the power. In (D) the broken front glass reduces the module current and power with a factor of 4. The IV curves of (E) and (F) have very similar shapes, indicating that the underlying defect is similar. The lower *short-circuit current* (Isc) value of (F) might be related to wafer quality from production and is not necessarily related to the thermal signature, supporting that (F) belong in category T1 rather than T2. Module (G) has a big step in the IV curve, indicating a crack, which also explains the colder 25% of the cell in the IRT image. This was confirmed by visual inspection, where a large crack was observed along the busbar of the upper hot cell. (H) exhibits a smaller step in current and a shunt. During visual inspection, a burn mark could be observed at the hot point. The burn mark is not in direct proximity to the bus bar and is assumed to be caused by a shunt in the cell. Consequently, the step in the IV curve is caused by the T1 signature at the top of the middle substring of the module, while the shunt is due to the T2/T3 combination in the right substring. Because of their low temperature, the additional T1's within the right substring is assumed to have little impact on the IV curve.

Fig. 3 shows the Mpp values for all modules containing a thermal signature, allowing us to quantify how defects within each category evolves over time. Note that several modules are classified into more than one category. Hence, the mean of the modules that only have one thermal signature are plotted as the dashed horizontal lines.

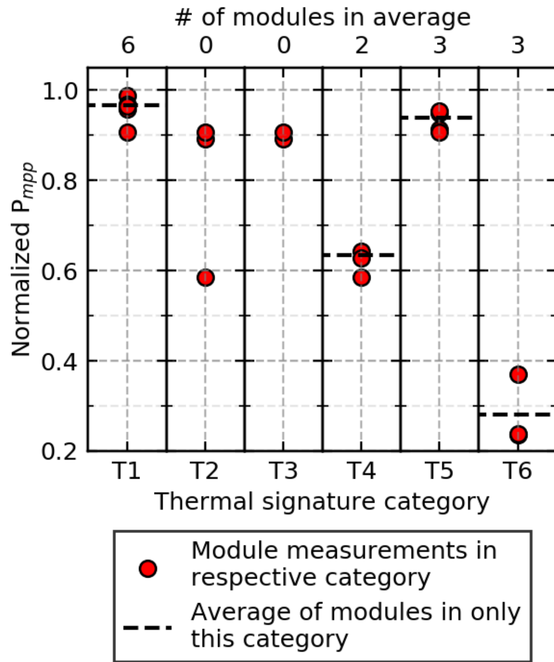

Figure 3: The Mpp points of all IV measurements done on modules within the 6 categories. Some modules are classified to more than one category, and do not contribute to the calculated average normalized power for the thermal signature classes. In total 18 modules were IV traced.

3.3 Circuit modeling

3.3.1 Equivalent circuits for defect parameterization

Module (A) was fitted and parameterized using the circuit model described in section 2.3, and the resulting five parameterization values are listed in Table 2. These parameters were used for all the simulated, non-defective modules. For simplicity, Is and Iph0 were kept constant in all further simulations.

Table 3: The parameterization resulting from fitting the circuit model to module (A) in Fig. 1 and 2.

5 parameter solar cell parameterization of the healthy module	
Diode saturation current, Is	6.3e-10 A
Solar-generated current, Iph0	8.045 A
Irradiance, Ir0	1000 W/m^2
Quality factor, N	1.0
Series resistance, Rs	8e-3 Ω

Because module (E) and (F) are assumed to have the same defect, modules (B)-(H), excepting (F), were fitted to the measured IV curves of Fig. 2. The resulting fits are shown in Fig. 4. The resulting parametrizations for the different thermal signatures are shown in Table 4.

Table 4: The parameterization of the model fitting to the IV traces in Fig. 4. L, M and R is short for the Left, Middle and Right substring, respectively.

Module	Irradiance reduction	Additional series resistance	Shunt resistance
(B)	-	R: 100 Ω	-
(C)	-	0.27 Ω outside substrings	-
(D)	L & M: 0.3, R: 0.23	-	M: 61 Ω, R: 35 Ω
(E)	R one cell: 0.87	-	R one cell: 6.5 Ω
(G)	R two cells: 0.75	R each of the two cells: 0.062 Ω	R each of the two cells: 25 Ω
(H)	M one cell: 0.88, R one cell: 0.75	-	M one cell: 27 Ω, R one cell: 9 Ω

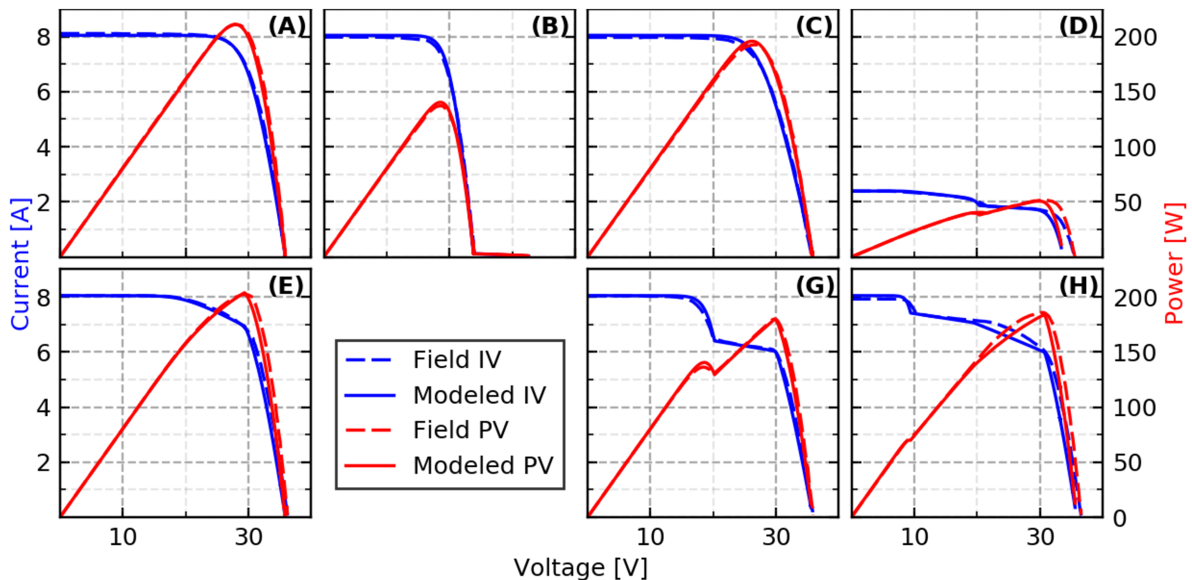

Figure 4: Fitting of model to IV trace. An irradiance reduction factor, a shunt resistance and additional series resistance were used to fit the IV trace of the thermal signatures in Fig 1 and 2. (F) was excluded because it displays similar IV characteristics as (E).

For (E), an irradiance reduction factor was necessary to emulate the slope close to Mpp, but no signs of cracks were visible in IRT. Similarly, for (G) a shunt resistor had to be added to get the slope in the step of the IV curve correct. In addition, the two T1 signatures in the right substring in (H) are assumed to have low impact on the IV characteristics compared to the T2/T3 defect and are consequently not included in the simulation.

3.3.2 String modeling

With the parametrization of the thermal signatures, it was possible to model how they affect the Mpp of a string as a function of string length. Each of the simulated modules of Fig 4(B)-(H) is simulated together with an increasing number of non-defective modules and normalized with respect to the power of a string with equal length but containing only non-defective modules. The result can be seen in Fig. 5. The figure describes string lengths from 1 up to 25 modules. Generally, the normalized power of a given thermal signature approaches 1 as more non-defective modules are added to the string, since the ratio of defective to non-defective modules decreases. The defect of module (D) has by far the largest impact on the normalized power. With two modules in series the normalized power of module (D) is at 0.5, meaning that the entire defective module is bypassed at string lengths >1. Interestingly, at a string length of 3 modules, the normalized power of (B), (G) and (H) intersect. From three modules and more, (G) and (B) have the exact same relative power, signifying that there is no longer any contribution to the Mpp from the substring with the thermal signature in (G), and the bypass diode activates. In addition, (H) degrades compared to the (B) and (G), despite having a higher Mpp at shorter string lengths. (C) and (E) show similar characteristics, with (C) slightly lower (0.93) than (E) (0.96) at low string lengths.

For string lengths above 12 modules the trend is similar. Interestingly, from around 18 modules in series and above the power loss of (B), (G), (H) and (D) become linear with respect to how many substrings within the defective modules that are affected by thermal signatures. At 19 modules in series the slope is -0.175 per affected substring. The slope of this function decreases with modules in series and at 25 it is about -0.133 per affected substring.

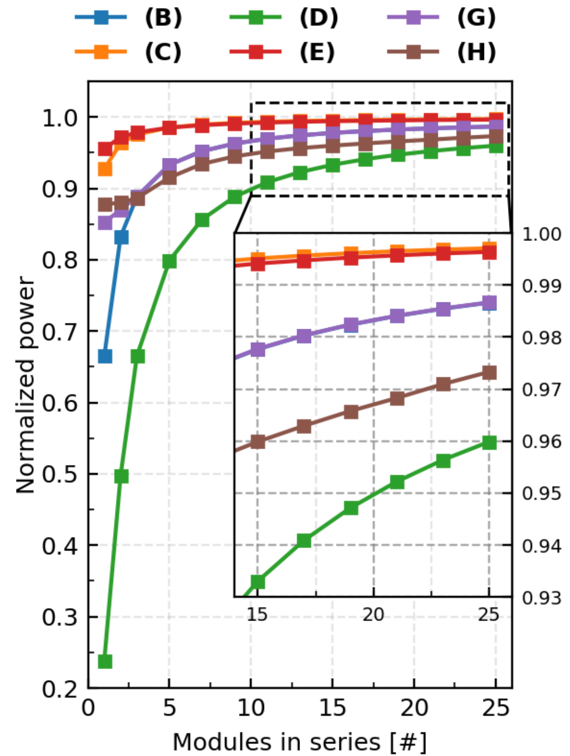

Figure 5: The power of a string with one of the defective modules and the rest (A) modules, as a function of string length, normalized to a string of equal length containing only (A) modules.

4 DISCUSSION

The current system for categorizing thermal signatures is adequate, but combined cases of T1 – T3 can be hard to classify. To more accurately categorize these, more statistics is needed. Especially important is which thermal gradients are needed within a cell to distinguish T1 from T2, as well as at which point T3 becomes more important than a T2 within the same cell. The relevant metric for this is ultimately how the differences in temperature affects the power characteristics of the cells and subsequently the module.

IV tracing is a very useful tool for understanding how thermal signatures affect the module power. The resulting IV characteristics from module (A)-(D) is similar to what is expected. (E) and (F) are similar in IRT, indicating that the thermal gradient over the cell in (F) is not sufficient to categorize it in T2, and it has a T1 signature. Since no soiling was observed during visual inspection, and we assume that a crack is the only cell defect that can create a step in the IV curve (Fig. 2 (G)), then (G) is classified as T2. Whether the shunting that was parametrized by module modeling is caused by the hot points, or by the crack itself due to a contact between the n and p layers in the cell is not clear. Taking into account that an irradiance correction factor had to be used for (F), could indicate that a crack and a shunt can coincide. If the same assumption is transferred to module (H), the T1 in the middle substring is also a crack, but without a T2 signature, solely based on the irradiance reduction factor used in the simulation. This could indicate that either a certain width of the crack is needed, or that a certain area of the cell has to be isolated, in order for the thermal signature to become a T2. Ultimately this could indicate that a T1 signature can have both low impacts on string power, like in module (B), and higher impacts, like in module (H), where a module substring is bypassed.

The comparison of IV trace data with flash data of the same modules provides insight into how the defects evolve over time. This is especially the case for T1 and T5 signatures. We do not know when the thermal signatures appeared, but generally these defect categories may have a limited effect on module degradation over time.

The string modeling shows how the different thermal signatures will affect the string Mpp. The fact that module (G) outputs the same power as a T4 at 3 modules in series indicates that the bypass diode is activated. If this is the case, the T2 signature should not be visible in an IR image. Nonetheless, T2 is observed, and the origin could be that the imaged system has several strings in parallel, with one Mpp tracker of the entire system.

Hence, the system Mpp, not the string Mpp, determines the voltage each string is operated at, with all parallel strings experiencing the same voltage. This means that the system likely has a larger reduction in power since the voltage of all healthy strings is reduced to the Mpp voltage of the defective string, rather than running at the healthy strings Mpp voltage. Said in another way: In parallel systems, to be fully bypassed, the power loss from a defect needs to be higher than the gain from running all other healthy strings at Mpp. It follows from this argument that the system power loss introduced by a given thermal signature will be highly dependent on the system design. At the same time the simulation results indicate that a single cell defect never has a larger impact than a bypassed substring, as long as the bypass diode of the substring does not fail. A reliable and fast method for bypass diode evaluation, without having to open the junction box, remains elusive to us in literature. It does, however, seem likely that a bypass diode failure would produce a power loss large enough to be reliably detected by good production data monitoring techniques in most systems.

Lastly, in Ref. [10] the detection limit of a defect is set at 3%. With this value, in a series of 25 modules only T6 signatures will be identifiable, and only cases where 3 bypass diodes or more are active will be observable in production data analysis of 25 module string systems. For 20 modules in series (H) will be visible as well.

5 CONCLUSION

The modeling framework developed here can be used to create an arbitrary string design ranging from systems with module optimizers to large parallel systems. This is useful because differences in string length, the amount of strings in parallel and granularity of both power measurement points and Mpp tracking from one system to another, will lead to differences in normalized power loss of a given failure. The premise for discovering a defect by monitoring production data is, hence, also very dependent on system design.

In the studied sample volume T6 is the most immediate candidate for replacement. As it poses a serious health and safety risk as well as a substantial power loss the module should be replaced, or as it is generally bypassed, be disconnected from the rest of the string at first convenience, if no replacement is at hand. T4 gives a substantial loss and should be replaced if possible. T2 and T3 are hard to distinguish in terms of power loss and show loss values that could potentially be of the same magnitude as the T4. Performance data from the plant should be evaluated to check for a bypass diode failure. T1 signatures can have a varied impact on string power, and therefore the same actions should be taken for this signature as for T2 and T3. If this is generally true, splitting T1-T3 into separate categories has no operational benefit, and the three categories should be merged. T5 shows a small impact on power, which means it is a candidate for further monitoring if it is detected in a PV installation, but it probably does not require immediate action unless the temperature difference from the rest of the module is higher than observed here.

Generally, the more substrings that contain the thermal signatures T1, T2, T3, T4 and T6 within a module, the worse the string power output is going to be, and the higher the module should be prioritized in O&M schemes.

REFERENCES

[1] J. A. Tsanakas, L. Ha, and C. Buerhop, "Faults and infrared thermographic diagnosis in operating c-Si photovoltaic modules: A review of research and future challenges," *Renew. Sustain. Energy Rev.*, vol. 62, no. Supplement C, pp. 695–709, 2016.

[2] C. Buerhop *et al.*, "Verifying defective PV-modules by IR-imaging and controlling with module optimizers," *Prog. Photovoltaics Res. Appl.*, vol. 26, no. 8, pp. 622–630, Aug. 2018.

[3] M. B. Øgaard, Å. Skomedal, and J. H. Selj, "Performance Evaluation of Monitoring Algorithms for Photovoltaic Systems," (in press). *Proc. 36th Eur. Photovolt. Sol. energy Conf. Exhib. (EU PVSEC)*, 2019.

[4] Å. Skomedal, M. B. Øgaard, J. H. Selj, H. Haug, and E. S. Marstein, "General, Robust and Scalable Methods for String Level Monitoring in Utility Scale PV Systems," (in press). *Proc. 36th Eur. Photovolt. Sol. energy Conf. Exhib. (EU PVSEC)*, 2019.

[5] International Electrotechnical Commission, "Photovoltaic (PV) systems - Requirements for testing, documentation and maintenance - Part 3: Photovoltaic modules and plants - Outdoor infrared thermography," *Tech. Specif. 62446-3*, 2017.

[6] International Electrotechnical Commission, "Photovoltaic devices - Procedures for temperature and irradiance corrections to measured I-V characteristics," *IEC 60891*, 2009.

[7] C. Buerhop, M. Krause, T. Winkler, J. Hauch, C. Camus, and C. J. Brabec, "Influence of the Module Temperature on the Performance and EL-Image of Precracked PV-Modules," *Proc. 35th Eur. Photovolt. Sol. energy Conf. Exhib. (EU PVSEC)*, pp. 1147–1151, 2018.

[8] The MathWorks Inc, "MATLAB R2018a simulink." Natick, Massachusetts, United States, 2018.

[9] C. Buerhop, R. Weißmann, H. Scheuerpflug, R. Auer, and C. J. Brabec, "Quality control of PV-modules in the field using a remote-controlled drone with an infrared camera," *Proc. 27th Eur. Photovolt. Sol. energy Conf. Exhib. (EU PVSEC)*, pp. 3370–3373, 2012.

[10] M. Köntges *et al.*, "Review of Failures of Photovoltaic Modules," *IEA-Photovoltaic Power Syst. Program.*, pp. 1–140, 2014.